IEEE Access
Multidisciplinary ⋮ Rapid Review ⋮ Open Access Journal

Received January 12, 2020, accepted January 23, 2020, date of publication February 10, 2020, date of current version March 2, 2020.

Digital Object Identifier 10.1109/ACCESS.2020.2972981

Balanced-to-Balanced Gysel Filtering Power Divider With Arbitrary Power Division

MING LUO[1], (Member, IEEE), XIAO-HONG TANG[1], (Member, IEEE), DI LU[1], (Member, IEEE), YONG-HONG ZHANG[1], (Member, IEEE), YONG LIU[1], XIN XU[1], AND YU CAO[2]

[1]School of Electronic Science and Engineering, University of Electronic Science and Technology of China, Chengdu 611731, China
[2]Chengdu Tiger Microwave Technology Company, Ltd., Chengdu 610097, China

Corresponding author: Xin Xu (xindereck0512@163.com)

ABSTRACT This paper presents the balanced-to-balanced Gysel filtering power divider with arbitrary power division for first time. Based on the multicoupled series-resonator bandpass prototype network, a detailed theory analysis is presented and the corresponding design equations are concluded. Two filtering power dividers with the division ratio of 2 and 3 are realized using the half-wavelength resonator and the short-stub-loaded resonator. Finally, two example circuits are fabricated and measured for verification. The measured results show good agreement with the simulated and confirm the theory.

INDEX TERMS Balanced-to-balanced power divider, bandpass filtering response, arbitrary power division, Gysel power divider.

I. INTRODUCTION

The balanced RF circuit has been widely used in modern communication system due to its high immunity to noise compared with the single-ended circuit [1]. To construct the balanced RF receiver/transceiver circuit, the balanced filter and power divider, which present identical function with their single-ended counterparts for differential-mode (DM) signal and present suppression for common-mode (CM) signal, have been presented.

The balanced filter with single-band and dual-band bandpass response was presented in [2] and [3] respectively. In [4], a wideband balanced filter was reported by using coupled-line stubs/coupled-line stub-loaded resonators and the modified coupled feed-lines. A tunable balanced bandpass filter with constant bandwidth was proposed in [5]. Based on the balanced bandpass filter, the balanced-to-balanced diplexer was proposed in [6]. For the balanced-to-balanced (BTB) power divider, several researches were presented [7]–[11]. In [7], a BTB power divider was presented but without good isolation between the output ports. A BTB Willkinson power divider with good isolation between output ports was reported in [8] by Bin Xia. Then, Bin Xia developed a BTB Gysel power divider with arbitrary power division in [9]. In [10], a wideband BTB Willkinson power divider was proposed. In [11], a balanced power divider with tunable power division was proposed. Moreover, the other balanced passive components were also reported, such as the balanced coupler [12] and the balanced crossover [13].

In order to future compact the RF system, the filtering power divider (FPD) which integrates the functions of filter and power divider has been extensively studied. In [14], both the single- and dual-band filtering power dividers were both reported. In [15], a filtering power divider with ultra-wideband bandpass response was designed using transversal filtering transformer. A detailed design method of FPD with arbitrary power division was presented in [16] using even-order filter and traditional Willkinson power divider. In [17]–[19], A synthesis method for filtering power divider with arbitrary power division and arbitrary order bandpass response was proposed but without considering the isolation. A Gysel filtering power divider with arbitrary power division and high isolation between two output ports was presented in [20]. Moreover, the rat-race hybrid with bandpass response was reported [21] using the electromagnetically-coupled resonator. The isolation was achieved by using the inherent phase-shift between electronic- and magnetic-coupling.

For the balanced-to-balanced filtering power divider, it was firstly reported in [22] using the same coupling scheme

The associate editor coordinating the review of this manuscript and approving it for publication was Yuhao Liu.

as presented in [21]. In [22], the FPD was realized by three full-wavelength resonators and a half-wavelength resonator. The full-wavelength resonators work at second-order resonance and the half-wavelength resonator works at the first-order resonance. By using the different phase-shift between first-order and second-order resonance, which was presented in [23], the equivalent electronic coupling was achieved. This configuration has good isolation between two output ports but also has a large size because the resonators work at second-order resonance. In our previously research [24], the BTB filtering power divider was realized by half-wavelength resonator and short-stub-loaded resonator (SSLR). Compared with the research proposed in [22], it achieved compacter size and wider suppression for the common-mode signal. Moreover, several other BTB filtering power dividers were presented in [25]–[27]. In [25], a BTB filtering power divider was designed with hish output isolation only using two square patch resonators. In [26] and [27], a wideband and dual-band BTB filtering power divider were presented respectively with high frequency selectivity using similar structure. For the BTB filtering power divider with unequal power division, it was firstly presented in [28] using the same structure presented in [22]. Although a series of design equations are provided, the corresponding theoretical analysis was insufficient in [28].

In this paper, the balanced-to-balanced Gysel filtering power divider (BTB-GFPD) with arbitrary power division is researched and designed. The research is presented with detailed analysis and conclude the corresponding design equations through a series of derivation and demonstration. The design topology of the proposed BTB-GFPD is extended from the design scheme in [21], [22], [24]. At first, the design topology is studied based on multicoupled series-resonator bandpass prototype network and the design equations are concluded. Then the BTB-GFPD realized using half-wavelength resonator and SSLR is also studied. And the detailed realization principle is proposed. Two BTB-GFPDs with the division ration of 2 and 3, and center-frequency of 2.4GHz are implemented and measured. The measured results are presented. Finally, a discussion about the limitation of division ration is concluded.

II. THEORY ANALYSIS

Fig. 1 is the coupling scheme of the proposed BTB-GFPD. It consists of four resonators. When the input signal is excited at port 1, the output signal at port 2 and port 3 will have arbitrary power division, while port 4 is introduced as an insolation port. This coupling scheme is used in [22], [24] to realize the BTB Gysel filtering power divider with equal output power. In [22], [24], the FPDs have a symmetrical structure and can be analyzed by odd- and even-mode analysis method. To realize arbitrary power division, the proposed FPDs are unsymmetrical. So, the traditional odd- and even-mode analysis method could not be applied.

When the signal is excited at port 1, the proposed BTB-GFPD can be seen as a multicoupled series-resonator

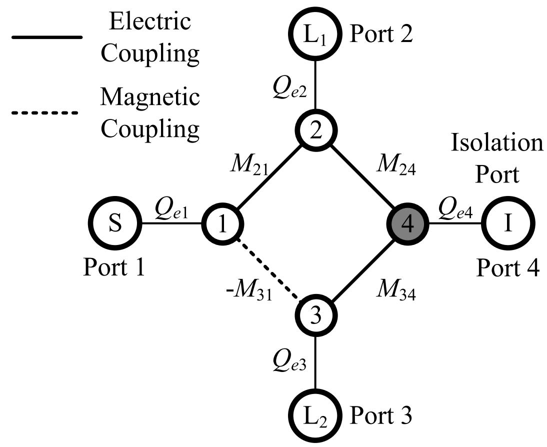

FIGURE 1. The coupling scheme of the proposed component.

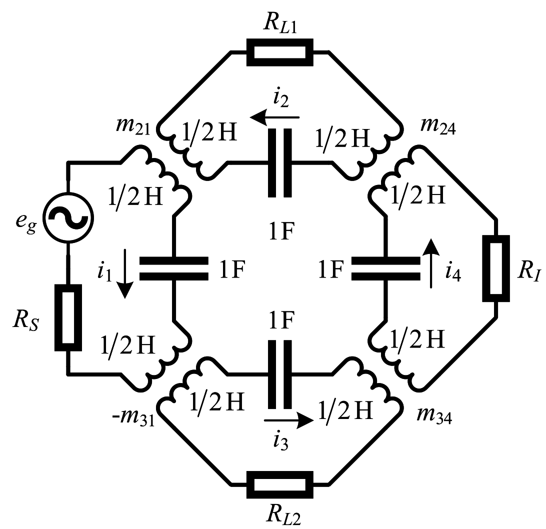

FIGURE 2. The multicoupled series-resonator bandpass prototype network of the proposed componet

bandpass prototype network in Fig. 2. It is attained by normalization of center-frequency and bandwidth as follow [29]:

$$\begin{bmatrix} m_{21} \\ m_{24} \\ m_{31} \\ m_{34} \end{bmatrix} = \frac{1}{FBW} \begin{bmatrix} M_{21} \\ M_{24} \\ M_{31} \\ M_{34} \end{bmatrix} \quad \begin{bmatrix} R_S \\ R_{L1} \\ R_{L2} \\ R_I \end{bmatrix} = \frac{1}{FBW} \begin{bmatrix} 1/Q_{e1} \\ 1/Q_{e2} \\ 1/Q_{e3} \\ 1/Q_{e4} \end{bmatrix} \tag{1}$$

where FBW is the fractional bandwidth. According to the Kirchhoff's law, the loop voltage can be calculated by loop current as follow:

$$\begin{bmatrix} e_g \\ 0 \\ 0 \\ 0 \end{bmatrix} = \begin{bmatrix} R_S + js & jm_{21} & -jm_{31} & 0 \\ jm_{21} & R_{L1} + js & 0 & jm_{24} \\ -jm_{31} & 0 & R_{L2} + js & jm_{34} \\ 0 & jm_{24} & jm_{34} & R_I + js \end{bmatrix} \begin{bmatrix} i_1 \\ i_2 \\ i_3 \\ i_4 \end{bmatrix} \tag{2}$$

where the s is the bandpass frequency variable($s = w - 1/w$ and w is the frequency variable).

A. ISOLATION

As a Gysel power divider, the isolation between two output ports is important. In the design of traditional

Gysel power divider, the isolation is realized by loading a lumped resistor without producing extra signal loss. In the presented BTB-GFPD, the port 4 is introduced as an isolation port. An 50Ω matching load is connected to port 4 instead of using a lumped resistor to realize the isolation between two output ports. For avoiding the 50Ω matching load produces extra signal loss, the isolation between port 1 and port 4 must be achieved. This has been attained in the design and can be verified through measuring the transmission parameter between port 1 and port 4. The theory analysis about the isolation between port 1 and port 4, and the isolation between port 2 and port 3 are both provided in the following.

When the input signal is added into port 1, the response of proposed BTB-GFPD can be attained by solving (2). Then, the following equation can be extracted as:

$$\begin{bmatrix} jm_{21} & R_{L1}+js & 0 & jm_{24} \\ -jm_{31} & 0 & R_{L2}+js & jm_{34} \\ 0 & jm_{24} & jm_{34} & R_I+js \end{bmatrix} \begin{bmatrix} i_1 \\ i_2 \\ i_3 \\ i_4 \end{bmatrix} = 0 \quad (3)$$

By applying the Gaussian elimination method, the following equation can be attained:

$$\begin{aligned}(R_I+js+\frac{m_{24}^2}{R_{L1}+js}+\frac{m_{34}^2}{R_{L2}+js})i_4 \\ =(\frac{m_{31}m_{34}}{R_{L2}+js}-\frac{m_{21}m_{24}}{R_{L1}+js})i_1\end{aligned} \quad (4)$$

The equation (4) shows the relationship between i_1 and i_4. If the i_4 is always zero whatever the i_1 is, port 4 will isolated from port 1. Therefore, for the isolation between port 1 and port 4, the following condition should be satisfied.

$$\frac{m_{21}m_{24}}{R_{L1}+js}=\frac{m_{31}m_{34}}{R_{L2}+js} \quad (5)$$

The equation (5) is the condition for realizing the isolation between port 1 and port 4. At the center frequency of bandpass ($w = 1\ rad/s$), it can be simplified as follow:

$$\frac{m_{21}m_{24}}{R_{L1}}=\frac{m_{31}m_{34}}{R_{L2}} \quad (6)$$

The transmission parameter between port 2 and port 3 can be researched by repeating the above analysis process. Similarly, the isolation between port 2 and port 3 can be concluded by as:

$$\frac{m_{21}m_{31}}{R_S}=\frac{m_{24}m_{34}}{R_I} \quad (7)$$

If (6) and (7) are both satisfied, the isolation between two output ports will be achieved and the 50Ω matching load will not increase the insertion loss of the power divider.

B. BANDPASS RESPONSE AND POWER DIVISION

When the input signal is added into port 1, the output of port 2 and port 3 can be attained by solving (2). The following equation can be attained:

$$\begin{bmatrix} e_g \\ 0 \\ 0 \end{bmatrix} = \begin{bmatrix} R_S+js & jm_{21} & -jm_{31} & 0 \\ jm_{21} & R_{L1}+js & 0 & jm_{24} \\ -jm_{31} & 0 & R_{L2}+js & jm_{34} \end{bmatrix} \begin{bmatrix} i_1 \\ i_2 \\ i_3 \\ i_4 \end{bmatrix} \quad (8)$$

It can be expanded as follow:

$$\begin{bmatrix} e_g \\ 0 \\ 0 \end{bmatrix} = \begin{bmatrix} R_S+js & jm_{21} & -jm_{31} \\ jm_{21} & R_{L1}+js & 0 \\ -jm_{31} & 0 & R_{L2}+js \end{bmatrix} \begin{bmatrix} i_1 \\ i_2 \\ i_3 \end{bmatrix} + \begin{bmatrix} 0 \\ jm_{24} \\ jm_{34} \end{bmatrix} i_4 \quad (9)$$

When the condition (6) is satisfied, i_4 will always be zero whatever i_1 is. Therefore, (9) can be simplified as follow:

$$\begin{bmatrix} e_g \\ 0 \\ 0 \end{bmatrix} = \begin{bmatrix} R_S+js & jm_{21} & -jm_{31} \\ jm_{21} & R_{L1}+js & 0 \\ -jm_{31} & 0 & R_{L2}+js \end{bmatrix} \begin{bmatrix} i_1 \\ i_2 \\ i_3 \end{bmatrix} \quad (10)$$

(10) is a simplification for (8) when the condition (6) is satisfied. Meanwhile, (10) can be seen as the mathematical representation of the prototype network in Fig. 3. This means that the prototype network in Fig. 2 and the prototype network in Fig. 3 will have same response when a signal is excited at port 1 and the condition (6) is satisfied. Based on (10), i_2 and i_3 can be calculated as follow:

$$i_2=-\frac{jm_{21}}{R_{L1}+js}i_1 \quad i_3=\frac{jm_{31}}{R_{L2}+js}i_1 \quad (11)$$

According to the calculation of power, the output power of port 2 and 3 at the center frequency can be calculated as follow:

$$P_2=\frac{m_{21}^2}{R_{L1}}i_1^2 \quad P_3=\frac{m_{31}^2}{R_{L2}}i_1^2 \quad (12)$$

For achieving the power division of α^2 ($P_2/P_3 = \alpha^2$), the following condition should be satisfied.

$$\frac{m_{21}^2}{R_{L1}}=\alpha^2\frac{m_{31}^2}{R_{L2}} \quad (13)$$

According to (13), a simple formulas can be obtained.

$$m_{21}=\alpha m_{31} \quad R_{L1}=R_{L2} \quad (14)$$

Based on the simplified prototype network presented in Fig. 3, the coupling scheme can be further simplified as

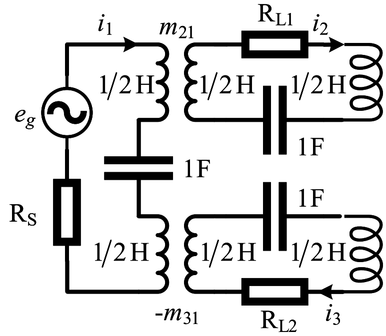

FIGURE 3. The simplified multicoupled series-resonator bandpass prototype network.

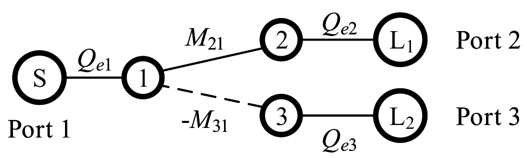

FIGURE 4. The simplified coupling scheme of the proposed component.

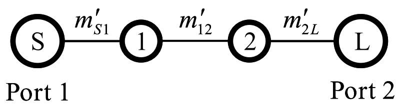

FIGURE 5. The traditional coupling prototype of second-order two-port bandpass filter.

Fig. 4. The simplified coupling scheme can be seen as a filtering power divider without isolation between two output ports, which has been detailed researched in [17], [18]. The Fig. 5 is the coupling prototype of traditional second-order two-port bandpass filter which can be synthesized according to the specifications of bandpass filtering response. The m'_{21} is its normalized internal coupling coefficient, and the m'_{s1} and m'_{2L} are both its normalized external coupling coefficients. For the proposed power divider, in order to realize the bandpass response, its coupling coefficient and external coupling parameters should satisfy the following condition as presented in [17], [18].

$$M_{21}^2 + M_{31}^2 = (m'_{21} \times FBW)^2 \tag{15}$$

$$Q_{e1} = \frac{1}{(m'_{S1})^2 \times FBW} \tag{16}$$

$$Q_{e2} = Q_{e3} = \frac{1}{(m'_{2L})^2 \times FBW} \tag{17}$$

III. REALIZABTION

The realization structure of this BTB-GFPD is shown in Fig. 6. It is constructed by half-wavelength resonator (HR) and short-stub-loaded resonator (SSLR) as presented in Fig. 1. The resonator 1, resonator 2 and resonator 3 are all HRs, and the resonator 4 is a SSLR. The HR and SSLR have been researched in [24]. In this section, a thorough discussion is presented.

A. COMMON-MODE SUPPRESSION

The structure of the HR with corresponding feeding line structure is provided in Fig. 7. Although, the whole component is unsymmetrical in order to realize unequal power division. Each HR and the corresponding feeding line are symmetrical. The dominant resonant frequency of HR (f_H) can be calculated as follow:

$$f_H = \frac{c}{2l_1\sqrt{\varepsilon_{ef}}} \tag{18}$$

where, c is the velocity of light in free space and ε_{ef} is the effective dielectric constant. The voltage distribution of dominant resonance is odd-symmetrical and also shown in Fig. 7. The electric coupling coefficient between HR and the feeding line k^e can be calculated as [30]

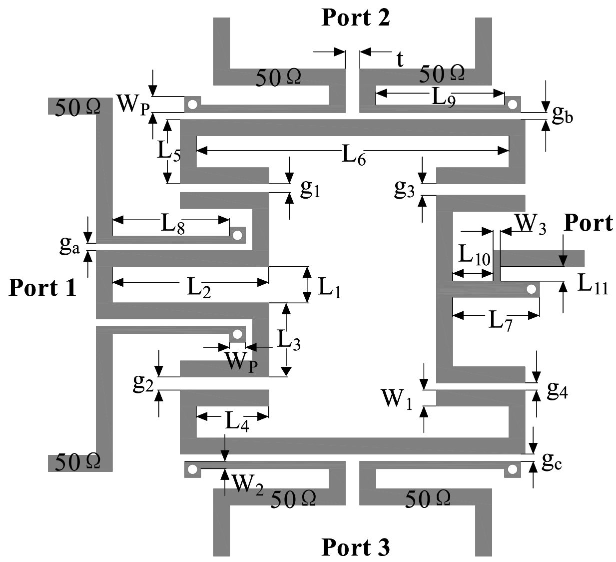

FIGURE 6. The structure of the proposed FPD.

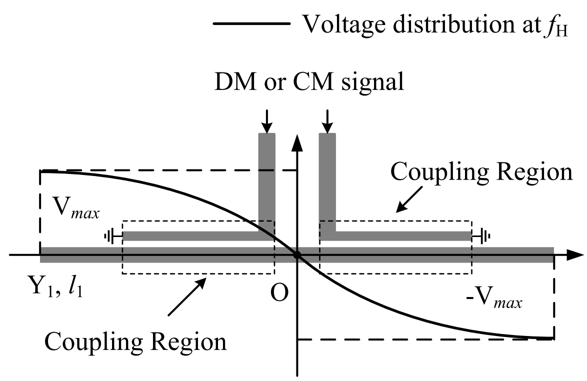

FIGURE 7. The structure of HR with corresponding feeding line structure and its field distribution of dominant resonance.

$$k^e = p \times \frac{\int_{CR} V_H(x)V_F(x)dx}{\sqrt{\int_{CR} |V_H(x)|^2 dx \times \int_{CR} |V_F(x)|^2 dx}} \tag{19}$$

where, CR represents the coupling region, $V_H(x)$ is voltage distribution of the dominant resonance of HR, $V_F(x)$ is voltage distribution of the feeding line and p represents a constant. As mentioned before, $V_H(x)$ is an odd function and the coupling region is symmetrical. When a CM signal is inserted, $V_F(x)$ will be a even function and k^e will be zero as a result. Similarly, the magnetic coupling coefficient k^m will be zero too when a CM signal is added. Therefore, CM input signal can not excite the dominant resonance of the HR. The HR is shut off for the CM signal. Thus, the suppression for CM signal is achieved.

B. EQUIVALENT MAGNETIC COUPLING

In the coupling scheme shown in Fig. 1, both electric and magnetic coupling are utilized to constructed the BTB-GFPD. The electric coupling and magnetic coupling have different phase shift in the transmission path which is

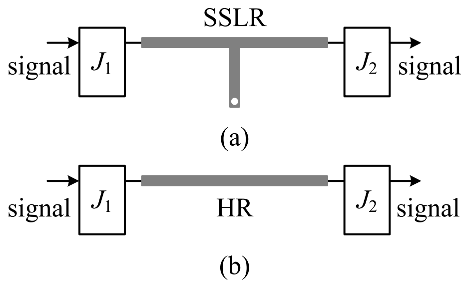

FIGURE 8. The schematic of signal transmission path: (a) SSLR (b) HR.

used to realize the isolation of the BTB-GFPD. However, in the practical realization, only the electric coupling exists between resonators. When a pair of signal pass through SSLR and HR respectively, a difference of 180° is existence between the phase shift of two transmission paths. This feature is used to equivalently realize magnetic coupling in the proposed BTB-GFPD.

Fig. 8(a) and 8(b) depicts a signal passing through SSLR and HR respectively. The J_1 and J_2 are admittance inverters which represent the electric coupling between resonators. Usually, they are with difference value. Their *ABCD* matrix T_1 and T_2 are as follow:

$$T_1 = \begin{bmatrix} 0 & j/J_1 \\ jJ_1 & 0 \end{bmatrix} \quad T_2 = \begin{bmatrix} 0 & j/J_2 \\ jJ_2 & 0 \end{bmatrix} \tag{20}$$

T_a and T_b is the *ABCD* matrix of transmission path a and b respectively. They can be calculated as:

$$T_a = \begin{bmatrix} A_a & B_a \\ C_a & D_a \end{bmatrix} = T_1 \times T_S \times T_2 \tag{21}$$

$$T_b = \begin{bmatrix} A_b & B_b \\ C_b & D_b \end{bmatrix} = T_1 \times T_H \times T_2 \tag{22}$$

where T_S and T_H is the *ABCD* matrix of SSLR and HR respectively. The SSLR has a symmetric structure shown in Fig. 9(a). Fig. 9(b) and 9(c) is its odd-mode and even-mode equivalent circuit model respectively. The input admittances of odd-mode equivalent circuit Y_S^{ino} and even-mode equivalent circuit Y_S^{ine} can be obtained as:

$$Y_S^{ino} = -jY_2 cot(2\pi f l_2 \sqrt{\varepsilon_{ef}}/c) \tag{23}$$

$$Y_S^{ine} = jY_2 \frac{2tan(2\pi f l_2 \sqrt{\varepsilon_{ef}}/c) - cot(2\pi f l_3 \sqrt{\varepsilon_{ef}}/c)}{2 + tan(2\pi f l_2 \sqrt{\varepsilon_{ef}}/c) cot(2\pi f l_3 \sqrt{\varepsilon_{ef}}/c)} \tag{24}$$

The *ABCD* matrix of SSLR T_S can be attained as follow [31]:

$$T_S = \begin{bmatrix} A_S & B_S \\ C_S & D_S \end{bmatrix} = \begin{bmatrix} \dfrac{Y_S^{ino} + Y_S^{ine}}{Y_S^{ino} - Y_S^{ine}} & \dfrac{2}{Y_S^{ino} - Y_S^{ine}} \\ \dfrac{2Y_S^{ino} Y_S^{ine}}{Y_S^{ino} - Y_S^{ine}} & \dfrac{Y_S^{ino} + Y_S^{ine}}{Y_S^{ino} - Y_S^{ine}} \end{bmatrix} \tag{25}$$

The dominant resonant frequency of SSLR (f_S) is its even-mode resonance and can be obtained by solving the following euqtion:

$$Y_S^{ine} = 0 \tag{26}$$

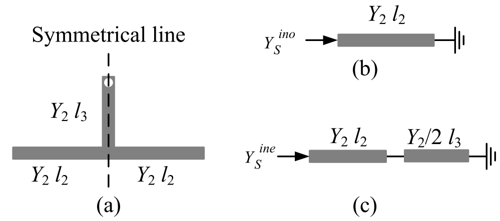

FIGURE 9. The structure and field distribution of half-wavelength resonator.

Therefore, The T_S can be simplified at the resonant frequency of f_S.

$$T_S = \begin{bmatrix} A_S & B_S \\ C_S & D_S \end{bmatrix} = \begin{bmatrix} 1 & \frac{2}{Y_S^{ino}} \\ 0 & 1 \end{bmatrix} \tag{27}$$

The HR has been widely studied in many literatures and its *ABCD* matrix T_H can be obtained in [29]. The dominant resonant frequency of HR (f_H) is its odd-mode resonance frequency. The T_H at the resonant frequency of f_H is as follow:

$$T_H = \begin{bmatrix} A_H & B_H \\ C_H & D_H \end{bmatrix} = \begin{bmatrix} -1 & 0 \\ 0 & -1 \end{bmatrix} \tag{28}$$

In this design, the HR and SSLR are with same dominant resonant frequency. The f_S and f_H are equal to the center-frequency of the passband (f_0). Using (21), (22), (27) and (28), the T_a and T_b can be obtained.

$$T_a = \begin{bmatrix} A_a & B_a \\ C_a & D_a \end{bmatrix} = \begin{bmatrix} J_2/J_1 & 0 \\ 2J_1J_2/Y_S^{ino} & J_1/J_2 \end{bmatrix}\Bigg|_{f=f_0} \tag{29}$$

$$T_b = \begin{bmatrix} A_b & B_b \\ C_b & D_b \end{bmatrix} = \begin{bmatrix} -J_2/J_1 & 0 \\ 0 & -J_1/J_2 \end{bmatrix}\Bigg|_{f=f_0} \tag{30}$$

Then, the transmission parameter at the center frequency f_0 of path a (S_a^{21}) and path b (S_b^{21}) can be calculated as follow:

$$S_a^{21} = \frac{2}{A_a + Y_0 B_a + \frac{C_a}{Y_0} + D_a} = \frac{2}{\frac{J_2}{J_1} + \frac{2J_1J_2}{Y_0 Y_S^{ino}} + \frac{J_1}{J_2}}\Bigg|_{f=f_0} \tag{31}$$

$$S_b^{21} = \frac{2}{A_b + Y_0 B_b + \frac{C_b}{Y_0} + D_b} = -\frac{2}{\frac{J_2}{J_1} + \frac{J_1}{J_2}}\Bigg|_{f=f_0} \tag{32}$$

where, Y_0 is the characteristic impedance of the terminal. In this design, Y_2 is set equal to Y_0. The second-order harmonic resonance of SSLR (f_S^{2th}) is approximately twice of f_S. Therefore,

$$Y_S^{ino}\Big|_{f=f_0} = -jY_2 cot(2\pi f l_2 \sqrt{\varepsilon_{ef}}/c)\Big|_{f=f_0} \approx -jY_2 = -jY_0 \tag{33}$$

For a bandpass filter with fractional bandwidth of 10%, the J_1/Y_0 and J_2/Y_0 are both with a very small value according [29]. So,

$$\frac{C_a}{Y_0}\Bigg|_{f=f_0} \approx j2\frac{J_1}{Y_0}\frac{J_2}{Y_0}\Bigg|_{f=f_0} \approx 0 \tag{34}$$

$$S_a^{21} \approx \frac{2}{\frac{J_2}{J_1} + \frac{J_1}{J_2}} = -S_b^{21} \tag{35}$$

The equation (35) indicates that the SSLR and HR have different phase shift in their transmission paths and the phase difference is 180°. In this way, equivalently-magnetic coupling (negtive coupling) $-M_{31}$ can be realized. Therefore, the BTB-GFPD can be constructed based on the coupling scheme in Fig. 1 using SSLR and HR.

IV. IMPLEMENT AND MEASUREMENT

Using ANSYS's HFSS, two BTB filtering powewr divider with the division ratio of 2 and 3 are designed on Rogers RO4350B with a permittivity of 3.48±0.05, loss tangent of 0.003 and thickness of 0.508*mm*. The corresponding coupling coefficients and external quality factors of the FPD with the division ratio of 2 are: $k_{21} = 0.0565$, $k_{31} = 0.0395$, $k_{24} = 0.0412$, $k_{34} = 0.0551$, $Q_{e1} = 21.86$, $Q_{e2} = 15.41$, $Q_{e3} = 15.41$ and $Q_{e4} = 18.07$. For the BTB-GFPD with the division ration of 3, its external quality factors are identical with the external quality factors of the BTB-GFPD with the division ratio of 2. Its coupling coefficients are as follow: $k_{21} = 0.0584$, $k_{31} = 0.0333$, $k_{24} = 0.0345$ and $k_{34} = 0.055$. Note here, all the presented BTB-GFPDs are measured by Keysight N524B network analyzer.

A. BTB-GFPD WITH THE DIVISION RATIO OF 2

Fig. 10 shows the response and photograph of the proposed BTB-GFPD with the division ratio of 2. Fig. 10(a) presents the transmission parameters of DM signal and CM signal. The simulated insertion loss for DM signal between port 2 and port 1, and between port 3 and port 1 is 2.78dB and 5.89dB respectively at the center-frequency of 2.4GHz with 3dB absolutely bandwidth of 214MHz and 3dB fractional bandwidth of 8.91%. The measured S_{dd21} is centered at 2.403GHz with the insertion loss of 3.12dB, 3dB absolutely bandwidth of 202MHz and 3dB fractional bandwidth of 8.41%. The center-frequency, insertion loss, 3dB absolutely bandwidth and 3dB fractional bandwidth of measured S_{dd31} is 2.404GHz, 6.21dB, 194MHz and 8.08% respectively. The S_{cc21} is <-50dB up to 4GHz in the simulation and is <-45dB up to 4GHz in the measurement. The simulated and measured S_{cc31} is <-51dB up to 4GHz and <-48dB up to 4GHz respectively.

This BTB-GFPD is designed with the power division of 2. Thus, the difference between S_{dd21} and S_{dd31} should be 3dB in theory. In simulation, this value is 3.11dB. In measurement, it is 3.09dB. The imbalance of magnitude of output power excluded the ideal difference of 3dB is presented in Fig. 10(e). The simulated imbalance of output power magnitude in passband is <0.16dB but the measured is <0.47dB. The deterioration is mainly caused by the manufacturing tolerance. The manufacturing tolerance generate the difference deviation both in center-frequency and bandwidth and also aggravates the imbalance of output power magnitude.

The Fig. 10(b) presents the isolation between port 2 and port 3 for the DM and CM signal. For the DM signal, the simulated isolation is >32dB and the measured isolation is >35dB. For the CM signal, the isolation is >64dB in simulation and >55dB in measurement. When a DM signal is added into port 1, the port 4 is isolated. The isolation performance is also presented in Fig. 10b which is >45dB in simulation and >34dB in measurement. For the common application, the 50Ω matched load can be replaced by a 50Ω lumped resistor. The isolation between port 4 and port 1 for DM signal guarantee the isolation resistor could not produce extra insertion loss. In the measurement, the isolation between port 2 and port 3 for the DM signal is improved but the isolation between port 4 and port 1 for the DM signal is deteriorated. This is mainly caused by the manufacturing tolerance.

The Fig. 10(c) shows the mode conversion between port 2 and port 1, and between port 3 and port 1. The simulated S_{dc21}, S_{cd21}, S_{dc31} and S_{cd31} are all <-50dB. But all of them are degraded in measurement. The measured S_{dc21} is <-31dB, the measured S_{cd21} is <-26dB, The measured S_{dc31} is <-36dB and the measured S_{cd31} is <-28dB. The mode conversion between port 2 and port 3 is shown in the Fig. 10(d). In simulation, the S_{dc32} and S_{cd32} are both <-60dB. In measurement, the S_{dc32} and S_{cd32} are both <-45dB.

The Fig. 10(f) shows the photograph of the proposed FPD with the division ratio of 2. Its dimensions are as follows (unit: *mm*): $L_1 = 1$, $L_2 = 10.8$, $L_3 = 4.1$, $L_4 = 5$, $L_5 = 3.41$, $L_6 = 21.6$, $L_7 = 6$, $L_8 = 8.4$, $L_9 = 8.4$, $L_{10} = 3.05$, $L_{11} = 1$, $W_1 = 1.1$, $W_2 = 0.25$, $W_3 = 0.25$, $W_p = 1.1$, $g_1 = 0.23$, $g_2 = 0.36$, $g_3 = 0.41$, $g_4 = 0.27$, $g_a = 0.17$, $g_b = 0.17$, $g_c = 0.17$, and t = 1. The diameter of vias are all 0.35*mm*. The effective size of this FPD is 23*mm*×30.6*mm* and $0.3\lambda_g \times 0.4\lambda_g$, where λ_g denotes the guided wavelength at 2.4 GHz.

B. BTB-GFPD WITH THE DIVISION RATIO OF 3

This BTB-GFPD is designed with the power division of 3. Its response and paragraph are all shown in Fig. 11. The transmission parameters of the DM and the CM signal is presented in the Fig. 11(a). The insertion loss for DM signal between port 2 and port 1 is 2.33dB in simulation and 2.66dB in measurement. The insertion loss for DM signal between port 3 and port 1 is 7.16dB in simulation and 7.46dB in measurement. The simulated S_{dd21} and S_{dd31} have the center-frequency of 2.4GHz, 3dB absolutely bandwidth of 203MHz and 3dB fractional bandwidth of 8.45%. For the measured S_{dd21}, the center-frequency, 3dB absolutely bandwidth and 3dB fractional bandwidth is 2.402GHz, 194MHz and 8.08% respectively. For the measured S_{dd31}, the center-frequency, 3dB absolutely bandwidth and 3dB fractional bandwidth is 2.404GHz, 194MHz and 8.07% respectively. The simulated S_{cc21} and S_{cc31} are both <-50dB up to 4GHz. In measurement, the S_{cc21} and S_{cc31} are both <-47dB up to 4GHz.

The ideal difference of S_{dd21} and S_{dd31} is 4.77dB when the division ratio is 3. The magnitude imbalance of output power excluded the ideal difference of 4.77dB is shown in Fig. 11(e). The simulated magnitude imbalance in passband is <0.1dB but the measured is <0.26dB.

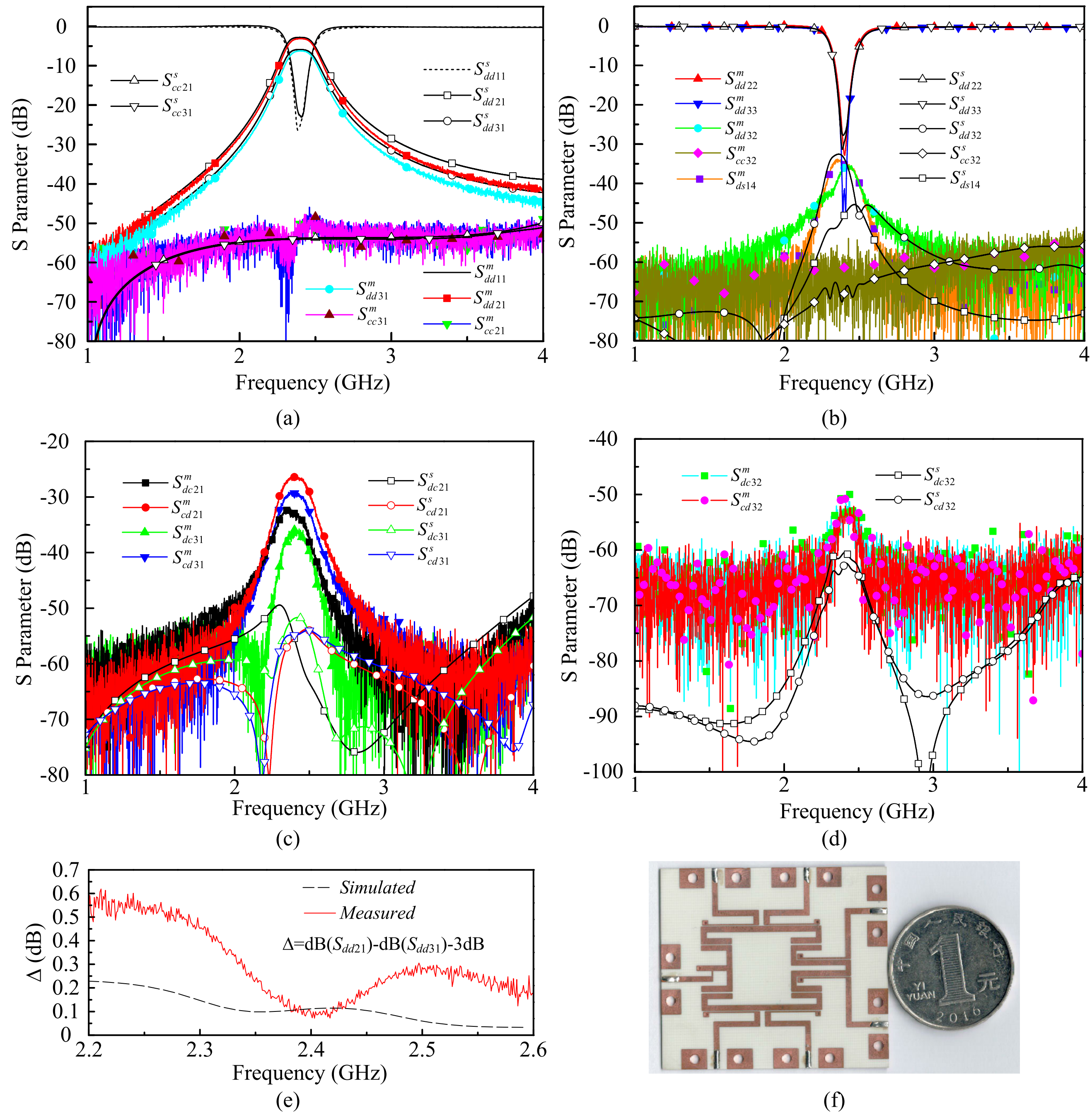

FIGURE 10. The simulated (with the superscript of *s*) and measured (with the superscript of *m*) results of the proposed FPD with the division ration of 2 and its photograph: (a) S_{dd11}, S_{dd21}, S_{dd31}, S_{cc21} and S_{cc31}; (b) S_{dd22}, S_{dd33}, S_{dd32}, S_{cc32} and S_{ds14}; (c) S_{dc21}, S_{cd21}, S_{dc31} and S_{cd31}; (d) S_{dc32} and S_{cd32}; (e) magnitude differences of differential-mode transmissions; (f) photograph.

The isolation between port 2 and port 3 and the isolation between port 4 and port 1 for the DM signal are presented in the Fig. 11(b). The simulated S_{dd32} and S_{cc32} is >30dB and >60dB respectively. But the measured S_{dd32} and S_{cc32} is >35dB and >55dB respectively. The isolation between port 4 and port 1 for DM signal S_{ds14} is >48dB in the simulation and is >40dB in the measurement.

Fig. 11(c) shows the mode conversion between port 2 and port 1, and between port 3 and port 1. The simulated S_{dc21}, S_{cd21}, S_{dc31} and S_{cd31} are all <-50dB. But the measured S_{dc21}, S_{cd21}, S_{dc31} and S_{cd31} is <-33dB, <-25dB, <-37dB and <-37dB respectively. The mode conversion between port 2 and port 3 is shown in the Fig. 11(d). In the simulation, the S_{dc32} and S_{cd32} are both <-59dB. In the measurement, the S_{dc32} is <-50dB and S_{cd32} is <-40dB.

Fig. 11(f) shows the photograph of the proposed FPD with the division ratio of 3. Its dimensions are as follows (unit: *mm*): $L_1 = 1, L_2 = 10.8, L_3 = 4.1, L_4 = 5, L_5 = 3.41, L_6 = 21.6, L_7 = 6, L_8 = 8.4, L_9 = 8.4, L_{10} = 3.05, L_{11} = 1, W_1 = 1.1, W_2 = 0.25, W_3 = 0.25, W_p = 1.1, g_1 = 0.22, g_2 = 0.43, g_3 = 0.49, g_4 = 0.26, g_a = 0.17, g_b = 0.17, g_c = 0.17$, and $t = 1$. The diameter of all vias are

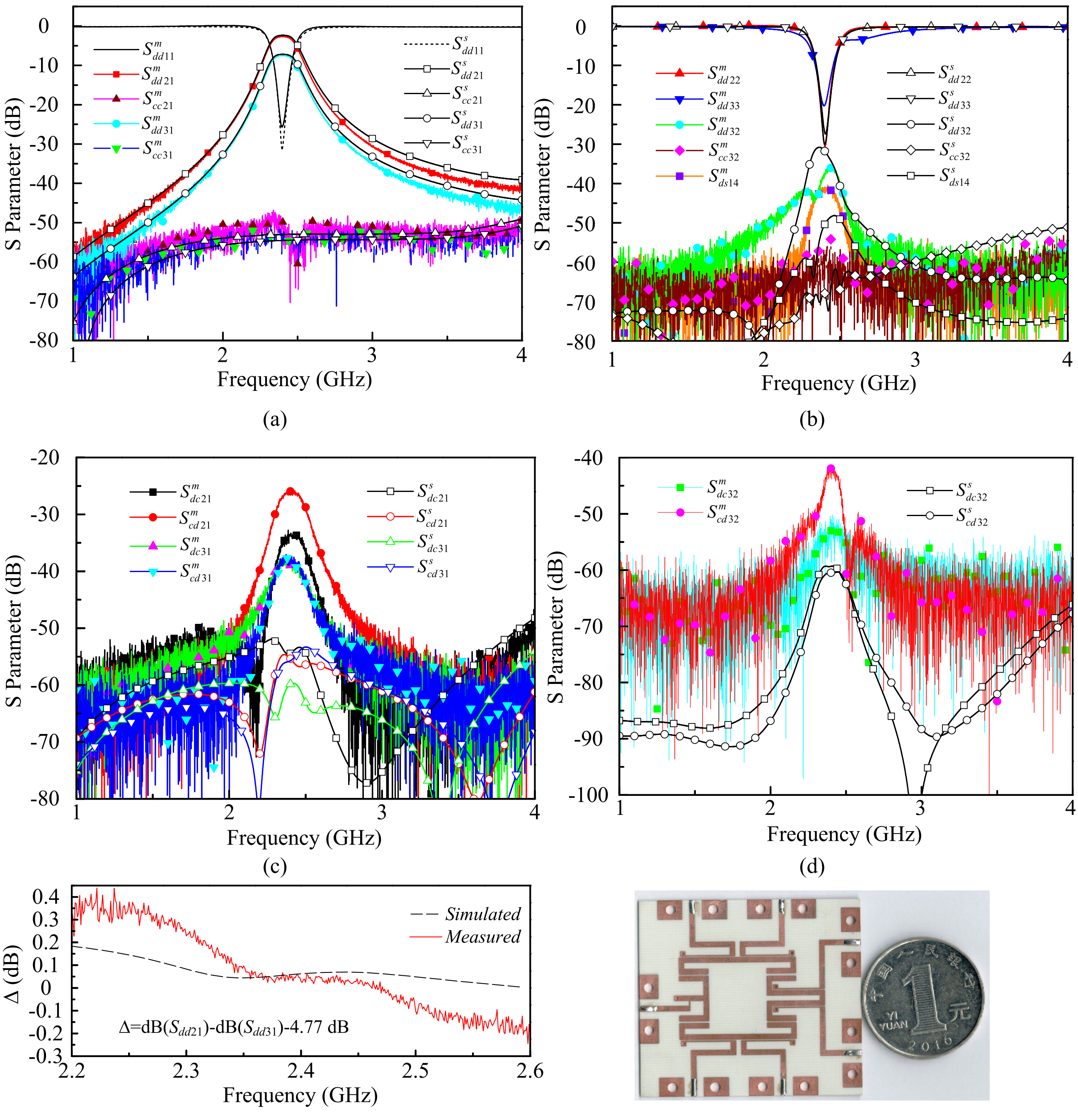

FIGURE 11. The simulated (with the superscript of *s*) and measured (with the superscript of *m*) results of the proposed FPD with the division ration of 3 and its photograph: (a)S_{dd11}, S_{dd21}, S_{dd31}, S_{cc21} and S_{cc31}; (b)S_{dd22}, S_{dd33}, S_{dd32}, S_{cc32} and S_{ds14}; (c)S_{dc21}, S_{cd21}, S_{dc31} and S_{cd31}; (d)S_{dc32} and S_{cd32}; (e)magnitude differences of differential-mode transmissions; (f)photograph.

0.35mm. The effective size of this FPD is 23.1$mm\times$30.6mm and $0.3\lambda_g\times0.4\lambda_g$, where λ_g denotes the guided wavelength at 2.4 GHz.

The measured isolation between two output ports of the designed FPDs are both >35dB and better than the isolation of the FPD presented in [28] which is only >16dB. This depends on the precise control for the external quality factor of resonator 4 (Q_{e4}) by adjusting the coupling strength between resonator 4 and the load. Furthermore, the FPD proposed in [28] was using the same structure presented in [22]. The structure of designed FPD in this paper is similar with the structure proposed in our previously research [24]. Thus, the designed FPDs in this paper keep the advantages in the suppression for common-mode signal and size compared with the FPD presented in [28].

V. FURTHER DISCUSSION ON THE DIVISION RATIO

According to (14), (15), (16) and (17), it can be concluded that the division ratio is determined by the internal coupling coefficient M_{21} and M_{31}, and the external coupling coefficient

Q_{e1}, Q_{e2} and Q_{e3} are all independent of the division ratio. For the designed two FPDs, they have different division ratio, but they have identical external coupling coefficients.

In the design, the division ratio α will be always larger than 1 if the output power P_2 is always larger than P_3. Then, the following equations can be obtained based on (13), (14) and (15).

$$0 \leq M_{31} \leq \frac{\sqrt{2}}{2} m'_{21} \times FBW \leq M_{21} \leq m'_{21} \times FBW \tag{36}$$

When M_{21} is equal to M_{31}, the output power P_2 is equal to P_3 and the division ratio α is 1. When M_{31} is zero, the output power P_3 is zero too and the division ratio α is infinity. So, the following equations can be attained obviously:

$$M_{21} = M_{31} = \frac{\sqrt{2}}{2} m'_{21} \times FBW \Rightarrow \alpha = 1 \tag{37}$$

$$\begin{cases} M_{21} = m'_{21} \times FBW \\ M_{31} = 0 \end{cases} \Rightarrow \alpha = \infty \tag{38}$$

The M_{31} can be regarded as zero if the g_2 is big enough. Therefore, the infinity of division ratio is achievable. Under this condition, the isolation between port 3 and port 2 and the isolation between port 4 and port 1 can be both achieved if the M_{24} is zero.

So, it is concluded that the arbitrary power division is achievable.

VI. CONCLUSION

This paper presents the balanced-to-balanced Gysel filtering power dividerwith arbitrary power division ratio. The coupling scheme is proposed and investigated based on multicoupled series-resonator bandpass prototype network. The corresponding design equations are also derived. The proposed FPDs are constructed by half-wavelength resonator and short-stub-loaded resonator. The detailed realization principle is also presented. For demonstration, two BTB filtering power dividers working at 2.4GHz with the power division of 2 and 3 are designed and measured. The results in measurement show good agreement with the simulation and verify the theory.

REFERENCES

[1] C.-H. Wang, Y.-H. Cho, C.-S. Lin, H. Wang, C.-H. Chen, D.-C. Niu, J. Yeh, C.-Y. Lee, and J. Chen, "A 60 GHz transmitter with integrated antenna in 0.18μm SiGe BiCMOS technology," in *IEEE Int. Solid-State Circuits Conf. (ISSCC) Dig. Tech. Papers*, Feb. 2006, pp. 659–668.

[2] P. Chu, W. Hong, K. Wang, H. Tang, Z. Hao, J. Chen, and K. Wu, "Balanced substrate integrated waveguide filter," *IEEE Trans. Microw. Theory Techn.*, vol. 62, no. 4, pp. 824–831, Apr. 2014.

[3] L. Yang, W.-W. Choi, K.-W. Tam, and L. Zhu, "Balanced dual-band bandpass filter with multiple transmission zeros using doubly short-ended resonator coupled line," *IEEE Trans. Microw. Theory Techn.*, vol. 63, no. 7, pp. 2225–2232, Jul. 2015.

[4] Q.-X. Chu and L.-L. Qiu, "Wideband balanced filters with high selectivity and common-mode suppression," *IEEE Trans. Microw. Theory Techn.*, vol. 63, no. 10, pp. 3462–3468, Oct. 2015.

[5] Y. C. Li and Q. Xue, "Tunable balanced bandpass filter with constant bandwidth and high common-mode suppression," *IEEE Trans. Microw. Theory Techn.*, vol. 59, no. 10, pp. 2452–2460, Oct. 2011.

[6] Y. Zhou, H.-W. Deng, and Y. Zhao, "Compact balanced-to-balanced microstrip diplexer with high isolation and common-mode suppression," *IEEE Microw. Wireless Compon. Lett.*, vol. 24, no. 3, pp. 143–145, Mar. 2014.

[7] J. W. May and G. M. Rebeiz, "A 40-50-GHz SiGe 1:8 differential power divider using shielded broadside-coupled striplines," *IEEE Trans. Microw. Theory Techn.*, vol. 56, no. 7, pp. 1575–1581, Jul. 2008.

[8] B. Xia, L.-S. Wu, and J. Mao, "A new balanced-to-balanced power divider/combiner," *IEEE Trans. Microw. Theory Techn.*, vol. 60, no. 9, pp. 2791–2798, Sep. 2012.

[9] B. Xia, L.-S. Wu, S.-W. Ren, and J.-F. Mao, "A balanced-to-balanced power divider with arbitrary power division," *IEEE Trans. Microw. Theory Techn.*, vol. 61, no. 8, pp. 2831–2840, Aug. 2013.

[10] J. Shi, J. Wang, K. Xu, J.-X. Chen, and W. Liu, "A balanced-to-balanced power divider with wide bandwidth," *IEEE Microw. Wireless Compon. Lett.*, vol. 25, no. 9, pp. 573–575, Sep. 2015.

[11] Y. Xiao, F. Lin, H. Ma, X. Tan, and H. Sun, "A planar balanced power divider with tunable power-dividing ratio," *IEEE Trans. Microw. Theory Techn.*, vol. 65, no. 12, pp. 4871–4882, Dec. 2017.

[12] J. Shi, J. Qiang, K. Xu, and J.-X. Chen, "A balanced branch-line coupler with arbitrary power division ratio," *IEEE Trans. Microw. Theory Techn.*, vol. 65, no. 1, pp. 78–85, Jan. 2017.

[13] Y.-H. Pang, E. D. Lin, and Y.-Y. Chen, "A planar balanced crossover," *IEEE Trans. Microw. Theory Techn.*, vol. 64, no. 6, pp. 1812–1821, Jun. 2016.

[14] Y. C. Li, Q. Xue, and X. Y. Zhang, "Single- and dual-band power dividers integrated with bandpass filters," *IEEE Trans. Microw. Theory Techn.*, vol. 61, no. 1, pp. 69–76, Jan. 2013.

[15] Y. Cao, X. Tang, and L. Wang, "A compact ultra-wideband power divider with favorable selectivity using transversal filtering transformer," *IEICE Electron. Exp.*, vol. 12, no. 12, 2015, Art. no. 20150427.

[16] P.-H. Deng and L.-C. Dai, "Unequal Wilkinson power dividers with favorable selectivity and high-isolation using coupled-line filter transformers," *IEEE Trans. Microw. Theory Techn.*, vol. 60, no. 6, pp. 1520–1529, Jun. 2012.

[17] T. Skaik, M. Lancaster, and F. Huang, "Synthesis of multiple output coupled resonator circuits using coupling matrix optimisation," *IET Microw. Antennas Propag.*, vol. 5, no. 9, p. 1081, 2011.

[18] K. Song, F. Chen, F. Zhang, and Y. Fan, "Synthesis and design method of bandpass-response power divider," *Microelectron. J.*, vol. 45, no. 1, pp. 71–77, Jan. 2014. [Online]. Available: http://www.sciencedirect.com/science/article/pii/S0026269213002292

[19] X. Yu and S. Sun, "Synthesis of filtering power divider with complex source and load impedances," in *Proc. IEEE Int. Symp. Antennas Propag. (APSURSI)*, Jun. 2016, pp. 1719–1720.

[20] K.-X. Wang, X. Y. Zhang, and B.-J. Hu, "Gysel power divider with arbitrary power ratios and filtering responses using coupling structure," *IEEE Trans. Microw. Theory Techn.*, vol. 62, no. 3, pp. 431–440, Mar. 2014.

[21] H. Uchida, N. Yoneda, Y. Konishi, and S. Makino, "Bandpass directional couplers with electromagnetically-coupled resonators," in *Proc. 2006 IEEE MTT-S Int. Microw. Symp. Dig.*, Jun. 2006, pp. 1563–1566.

[22] L.-S. Wu, Y.-X. Guo, and J.-F. Mao, "Balanced-to-balanced Gysel power divider with bandpass filtering response," *IEEE Trans. Microw. Theory Techn.*, vol. 61, no. 12, pp. 4052–4062, Dec. 2013.

[23] U. Rosenberg and S. Amari, "Novel coupling schemes for microwave resonator filters," *IEEE Trans. Microw. Theory Techn.*, vol. 50, no. 12, pp. 2896–2902, Dec. 2002.

[24] M. Luo, X. Xu, X.-H. Tang, and Y.-H. Zhang, "A compact balanced-to-balanced filtering Gysel power divider using $\lambda_g/2$ resonators and short-stub-loaded resonator," *IEEE Microw. Wireless Compon. Lett.*, vol. 27, no. 7, pp. 645–647, Jul. 2017.

[25] Q. Liu, J. Wang, L. Zhu, G. Zhang, and W. Wu, "Design of a new balanced-to-balanced filtering power divider based on square patch resonator," *IEEE Trans. Microw. Theory Techn.*, vol. 66, no. 12, pp. 5280–5289, Dec. 2018.

[26] F. Wei, Z.-J. Yang, P.-Y. Qin, Y. J. Guo, B. Li, and X.-W. Shi, "A balanced-to-balanced in-phase filtering power divider with high selectivity and isolation," *IEEE Trans. Microw. Theory Techn.*, vol. 67, no. 2, pp. 683–694, Feb. 2019.

[27] L. Chen, F. Wei, X. Y. Cheng, and Q. K. Xiao, "A dual-band balanced-to-balanced power divider with high selectivity and wide stopband," *IEEE Access*, vol. 7, pp. 40114–40119, 2019.

[28] B.-Y. Wang, X.-Y. Wang, L.-S. Wu, and J.-F. Mao, "A balanced-to-balanced filtering Gysel power divider with unequal power division," in *Proc. 6th Asia–Pacific Conf. Antennas Propag. (APCAP)*, Oct. 2017, pp. 1–3.

[29] R. J. Cameron, C. M. Kudsia, and R. R. Mansour, *Microwave Filters for Communication Systems: Fundamentals, Design, and Applications*. Hoboken, NJ, USA: Wiley, 2007.

[30] X.-L. Zhao, L. Gao, X. Y. Zhang, and J.-X. Xu, "Novel filtering power divider with wide stopband using discriminating coupling," *IEEE Microw. Wireless Compon. Lett.*, vol. 26, no. 8, pp. 580–582, Aug. 2016.

[31] I. Hunter, *Theory and Design of Microwave Filters*. Edison, NJ, USA: IET, 2001, no. 48.

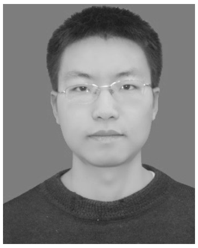

MING LUO (Member, IEEE) received the M.S. degree in electromagnetism and microwave technology from the University of Electronic Science and Technology of China (UESTC), Chengdu, China, in 2014, where he is currently pursuing the Ph.D. degree. His research interests include microwave and mm-wave circuits and systems.

XIAO-HONG TANG (Member, IEEE) received the B.S. and Ph.D. degrees in electromagnetism and microwave technology from the University of Electronic Science and Technology of China (UESTC). He is currently a Professor with UESTC. He has authored more than 100 journals and conference papers. His research interests include microwave and millimeter communication and computational electromagnetics. He was also a recipient of several national and provincial awards.

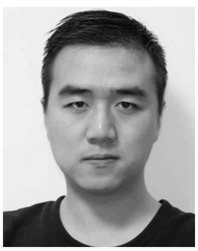

DI LU (Member, IEEE) received the M.S. degree from the Chengdu University of Information and Technology, in 2013, and the Ph.D. degree from the University of Science and Technology of China (UESTC), in 2018.

From 2015 to 2017, he was a Visiting Staff with the University of Virginia, Charlottesville, VA, USA. He is currently a Postdoctoral Researcher with The Chinese University of Hong Kong, Hong Kong. His main research interests include the design of MMIC microwave passive circuit, tunable circuit, frequency multipliers, mixers, millimeter-wave circuits, and RF MEMS.

YONG-HONG ZHANG (Member, IEEE) received the B.S., M.S., and Ph.D. degrees from the University of Electronic Science and Technology of China (UESTC), Chengdu, China, in 1992, 1995, and 2001, respectively.

From 1995 to 2002, he was a Lecturer with the School of Electronic Science and Engineering, UESTC. From 2002 to 2004, he was a Postdoctoral Fellow with the Department of Electronic Engineering, Tsinghua University, Beijing, China. Since 2004, he has been with UESTC, where he is currently a Full Professor. His research interests include microwave and millimeter-wave technology and applications. He is a Senior Member of the Chinese Institute of Electronics.

YONG LIU received the B.S. and Ph.D. degrees in electromagnetism and microwave technology from the University of Electronic Science and Technology of China (UESTC). He is currently a Research Associate with UESTC. He has authored more than 15 journals and conference papers. His research interests include microwave and millimeter-wave communication and circuit system design.

XIN XU received the B.S. and Ph.D. degrees in electromagnetism and microwave technology from the University of Electronic Science and Technology of China (UESTC), Chengdu, China, in 2007 and 2015, respectively. In 2015, he joined the School of Electronic Science and Engineering, UESTC, as a Research Assistant. He is currently a Visiting Scholar with the Communication Electronics Research Group, Linköping University, Sweden. His research interests include microwave and mm-wave circuits and systems.

YU CAO received the B.S. degree from the Southwest University of Science and Technology (SWUST), China, in 2006, and the M.Eng. degree from the University of Electronic Science and Technology of China (UESTC), China, in 2015. Since 2015, he has been the Research and Development Director with the Communication BU, Chengdu Tiger Microwave Technology, Company, Ltd. His research area includes microwave/millimeter wave circuit design.